APPENDIX M

COLD-TRAP EFFECTS
(RESPONSE TO TEF 2.05 AND GEN 1.01 (COMMENTS 5 AND 16))

Note Regarding the Status of Supporting Technical Information

This document was prepared using the most current information available at the time of its development. This Technical Basis Document and its appendices providing Key Technical Issue Agreement responses that were prepared using preliminary or draft information reflect the status of the Yucca Mountain Project's scientific and design bases at the time of submittal. In some cases this involved the use of draft Analysis and Model Reports (AMRs) and other draft references whose contents may change with time. Information that evolves through subsequent revisions of the AMRs and other references will be reflected in the License Application (LA) as the approved analyses of record at the time of LA submittal. Consequently, the Project will not routinely update either this Technical Basis Document or its Key Technical Issue Agreement appendices to reflect changes in the supporting references prior to submittal of the LA.

APPENDIX M

COLD-TRAP EFFECTS (RESPONSE TO TEF 2.05 AND GEN 1.01 (COMMENTS 5 AND 16))

This appendix provides a response for Key Technical Issue (KTI) agreement Thermal Effects on Flow (TEF) 2.05 and General Agreement (GEN) 1.01 (Comments 5 and 16). Agreement TEF 2.05 relates to the understanding of cold-trap effects and their treatment in model abstractions.

M.1 KEY TECHNICAL ISSUE AGREEMENTS

M.1.1 TEF 2.05

Agreement TEF 2.05 was reached during the U.S. Nuclear Regulatory Commission (NRC)/U.S. Department of Energy (DOE) Technical Exchange and Management Meeting on Thermal Effects on Flow held January 8 to 9, 2001, in Pleasanton, California (Reamer and Williams 2001). TEF subissues 1 and 2 were discussed at the meeting. There has been no submittal to the NRC related to this KTI agreement.

Agreement GEN 1.01 was reached during the NRC/DOE Technical Exchange and Management Meeting on Range of Thermal Operating Temperatures, held September 18 to 19, 2001 (Reamer and Gil 2001). At that meeting, the NRC provided additional comments that relate to TEF 2.05. These resulted in GEN 1.01 (Comments 5 and 16), and the DOE provided an initial response to those comments (Reamer and Gil 2001).

The wording of the agreements is as follows:

TEF 2.05

> Represent the cold-trap effect in the appropriate models or provide the technical basis for exclusion of it in the various scale models (mountain, drift, etc.) considering effects on TEF and other abstraction/models (chemistry). See page 11 of the Open Item (OI) 2 presentation. The DOE will represent the "cold-trap" effect in the *Multi-Scale Thermohydrologic Model* AMR (ANL-EBS-MD-00049) Rev 01, expected to be available in FY 02. This report will provide technical support for inclusion or exclusion of the cold-trap effect in the various scale models. The analysis will consider thermal effects on flow and the in-drift geochemical environment abstraction.

GEN 1.01 (Comment 5)

> DOE did not adequately assess the probability and effects of condensation forming under the drip shield for the LTOM.

DOE Initial Response to GEN 1.01 (Comment 5)

The repository performance is not sensitive to the uncertainty in condensation under the drip shield for the current LTOM results. The effect of LTOM calculations will tend to not have a significant impact since substantial waste package failure will not occur during the period when significant evaporation and condensation will occur. In addition, the bounding model ignores several effects that will reduce the flux from condensation, such as (1) natural convection lowering the temperature difference between drip shield and invert, and (2) the potential for condensation on cooler elements of the EBS, such as the vertical sides of the drip shield or the drift walls.

KTI agreement TEF 2.5 and FEP 2.1.08.14.00, Condensation on the underside of the drip shield addresses this concern.

GEN 1.01 (Comment 16)

Closed drifts will have RH close to 1.0. Small temperature gradients in this environment may result in convection, vapor transport, and dripping from condensation. This provides a pathway for water to enter the drift, by vapor exchange at the driftwall, and drip onto engineered materials. Presently the DOE considers convection and condensation in a drift cross-section but does not consider convection along the drift axis.

Basis:

Agreement TEF 2.05 addresses condensation generally under the heading of cold-trap effect. This agreement specifically addresses lateral flow of vapor along the drift axis in response to temperature gradients such as those created by the edge-effect. This process may be responsible for the dripping observed in the sealed ECRB drift.

DOE Initial Response to GEN 1.01 (Comment 16)

The DOE plans to investigate the observations of moisture in the ECRB bulkhead test consistent with existing agreement TSPAI.3.07. Measurements of pore-water moisture tension, relative humidity, and temperature combined with modeling will be used to help interpret the observations. Model calculations will be performed to ensure that the seepage model is consistent with observations and will be used as part of the model validation. The condensation issue will be further investigated for the lower-temperature operating mode should DOE pursue this operating mode in a potential license application (see response to comment 14).

Existing agreement, TEF 2.05 “Represent the cold-trap effect in the appropriate models or provide the technical basis for exclusion of it in the various scale models (mountain, drift, etc.) considering effects on TEF and other

abstraction/models (chemistry). Page 11 of the Open Item (OI) 2 presentation" is relevant to this question.

M.1.2 Related Key Technical Issue Agreements

Agreement TEF 2.04 relates to TEF 2.05. Agreement TEF 2.04 provides a description of the multiscale thermal-hydrologic model. The multiscale thermal-hydrologic model calculates the in-drift thermal-hydrologic environment, primarily temperature on the in-drift components and relative humidity of the in-drift air.

M.2 RELEVANCE TO REPOSITORY PERFORMANCE

Cold traps are a potential source of vapor flow and transport in the drift and invert and can affect the in-drift thermal-hydrologic conditions (i.e., the amount of water available to contact the waste packages). Therefore, cold traps can potentially influence the long-term performance of the drip shield and waste package and any subsequent release or mobilization of radionuclides outside the engineered barrier system.

M.3 RESPONSE

Cold-trap condensation processes are partly included and partly excluded from the total system performance assessment for the license application (TSPA-LA). Cold-trap effects within the emplacement drift between the drift wall and the drip shield are represented in the TSPA-LA by the condensation model documented in *In-Drift Natural Convection and Condensation Model* (BSC 2003a). This is a network model that produces bounding estimates for the frequency and magnitude of condensation at waste package locations. Condensation on the drift walls is included in the TSPA-LA and is represented in the same manner as drift seepage, although with a different spatial distribution and flux rate. As such, it affects the transport of radionuclides through the drift invert and the partitioning of that transport into the fractures and matrix of the host rock. On the other hand, condensation on the underside of the drip shield is excluded from the TSPA-LA on the basis that it occurs infrequently, has limited magnitude, and results in minimal, if any, additional releases of radionuclides. The exclusion argument is further described in *Engineered Barrier System Features, Events, and Processes* (BSC 2004a, FEP 2.1.08.14.0A).

The condensation network model describes the frequency and magnitude of drift-wall condensation at waste package locations after the emplacement drift walls have cooled to below boiling (96°C). Stated differently, the gas-drive effect associated with water vapor partial pressures greater than the total pressure in the unheated parts of the drift, which can result when the host-rock temperature is greater than boiling, is not included in the condensation network model. Vapor transport and condensation during this period, which lasts for only a few hundred years after closure, are investigated using the three-dimensional porous-medium model discussed below and in *Multiscale Thermohydrologic Model* (BSC 2004b, Section 7.5). For implementation in the TSPA-LA, condensation at a particular waste package location becomes possible (but does not necessarily occur) when the local drift-wall temperature cools below boiling (96°C). Hotter waste package locations take longer to cool according to the output of the multiscale model (BSC 2004b), delaying the onset of potential condensation at those drift-wall

locations. Once a particular waste package representation in the TSPA-LA has cooled to below boiling, the occurrence of condensation is sampled from a statistical distribution, which is correlated with the local percolation flux.

A cold-trap effect also occurs within the host rock, at a smaller scale, in response to nonuniform heating by waste packages with different heat output (BSC 2004b, Section 7.5). The concern is that drift seepage could occur at the locations of cooler waste packages, caused by liquid flux shed from the rock above adjacent hotter waste packages. This cold-trap effect and related phenomena are represented using a three-dimensional, three-drift, thermal-hydrologic, porous-medium model, with different cases to evaluate alternative boundary conditions and the effect of vapor dispersivity in the drift air. Results from this model show that, whereas liquid flux is increased in the host rock above a colder waste package adjacent to a hotter one, the potential for drift seepage is already encompassed by the seepage abstraction that is implemented in the TSPA-LA. The potential for seepage due to condensation reflux within the host rock is small because (1) the duration and magnitude of the liquid flux above cooler waste packages are limited, (2) the local rock temperature is also increased by thermal radiation, and (3) the combined effects of elevated temperature and capillary diversion on potential seepage are included in the TSPA-LA (BSC 2004c, Section 6).

GEN 1.01 (Comments 5 and 16) is addressed in Section M.4, along with more detailed discussion of the foregoing response summary.

The information in this report is responsive to agreements TEF 2.05 and GEN 1.01 (Comments 5 and 16) made between the DOE and the NRC. The report contains the information that the DOE considers necessary for NRC review for closure of these agreements.

M.4 BASIS FOR THE RESPONSE

The following sections describe the porous-medium model and the condensation network model, present representative results, discuss cold-trap effects, and describe the screening argument for condensation under drip shields.

M.4.1 Porous-Medium Model and Results

Two types of models have been constructed to evaluate vapor transport, evaporation, and condensation along emplacement drifts. The first is a fully three-dimensional porous-medium model implemented using the NUFT code (Nitao 1998) that approximates flow in the emplacement drift using pseudoporous-media properties. The property values were developed, in part, on the basis of single-phase computational fluid dynamic model calculations (BSC 2004b, Section 7.5; BSC 2003a).

The objective of the evaluation is to determine if it is necessary to include cold-trap effects explicitly in the description of temperature and relative humidity in the emplacement drifts that is provided by the multiscale thermal-hydrologic model for use in the TSPA-LA. The porous-medium model to be discussed here consists of a three-drift test case representing a scaled-down repository. Each simulated drift is 243 m long and uses a line-averaged heat source to represent the waste packages. The central drift uses a combination of a line-averaged heat source for most of the drift and four discrete sources (representing individual waste packages) at

the outer end of the drift (Figure M-1). This three-drift model is called the discrete/line-averaged mountain-scale thermal-hydrologic (D/LMTH) model.

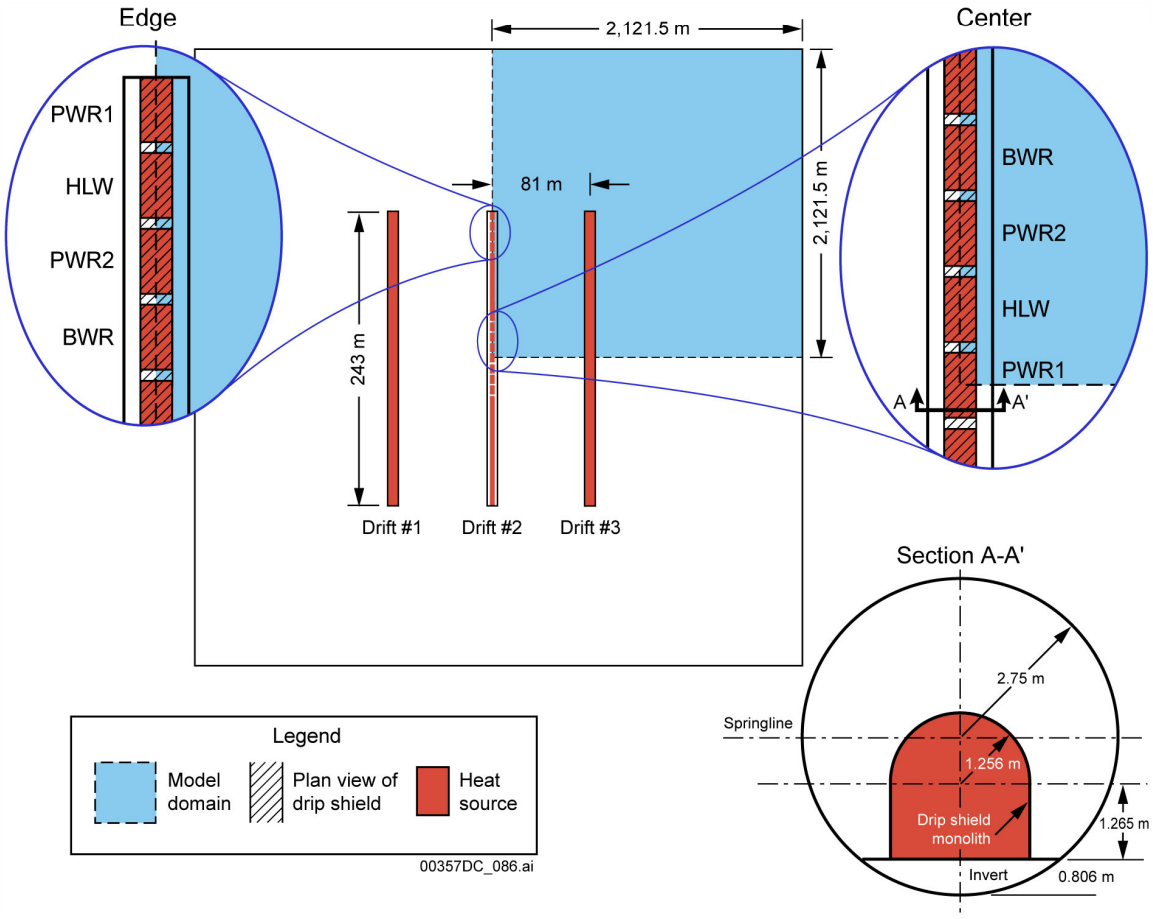

Source: BSC 2004b, Figure 7.5-1.

NOTE: To the upper left is the plan view of the three-drift repository system; highlighted in blue is the zone of symmetry. To the upper right is a close-up of the Drift #2 waste package sequencing. To the bottom right is the vertical cross section of the modeled drift with the drip shield and waste package lumped together as a heat source. This schematic depicts two models, with one model discretely representing the four waste packages at the repository center, and the second model discretely representing the four waste packages at the repository edge. The second model (representing the four waste packages at the edge) was used to evaluate the influence of the cold-trap effect.

Figure M-1. Schematic for the Multiscale Thermal-Hydrologic Model Validation Test Case

The D/LMTH model was run in three ways: (1) with no gas transport along the drifts, corresponding to the assumption in the multiscale thermal-hydrologic model of no significant gas transport along the drift axis; (2) with gas transport (using a small gas dispersion coefficient that accounts for binary diffusion of water vapor but not for the influence of convective mixing) and a bulkhead located just beyond the outermost waste package at the end of the drift; and (3) with gas transport (using a larger value of the gas dispersion coefficient to account for the influence of turbulent convective mixing) and no bulkhead at the end of the drift. The third case also includes the unheated section of the drift (turnout area) beyond the last outermost waste package, and it

includes the effects of rock dryout during the ventilation period (BSC 2004b, Section 7.5). Of the three D/LMTH model cases, the third is most realistic.

Comparison of the multiscale thermal-hydrologic model with the three D/LMTH cases is shown in Figures M-2 to M-4. Temperatures predicted by the D/LMTH cases (Figure M-2) clearly show that the effect of axial transport of vapor and condensation on temperatures is small. The multiscale thermal-hydrologic model overpredicts peak temperatures for the outermost two waste packages at the repository edge by about 15 C° (BSC 2004b, Section 7.5, Table 7.5-5). For the third and fourth waste packages in from the repository edge, the multiscale thermal-hydrologic model overpredicts peak temperatures by approximately 5 C° to 7 C° as compared to the D/LMTH cases. For waste packages located more than 20 m from the repository edge, which encompasses 97% of the repository area, the overprediction by the multiscale thermal-hydrologic model is less than 5 C°. The differences between the multiscale thermal-hydrologic model and the D/LMTH cases are related to how the multiscale thermal-hydrologic model addresses three-dimensional heat losses (BSC 2004b, Section 7.5).

Inclusion of axial vapor transport and the unheated part of the drift in the D/LMTH model (with no bulkhead and large dispersivity; i.e., case 3) improves the agreement of predicted relative humidity (Figure M-3) and liquid-phase saturation (Figure M-4) between the multiscale thermal-hydrologic model and the D/LMTH model. Note that the inclusion of the influence of host-rock dryout during the ventilation period (also case 3) has a very small effect on temperatures during the postclosure period (Figure M-2). It is also noted that the maximum bias of about 15 C° in the predicted temperatures at the repository edge (Figure M-2) is small compared to the effect of parametric uncertainty that is represented in the multiscale thermal-hydrologic model output used for the TSPA-LA (BSC 2004b, Sections 6.3.4 and 6.3.5).

Figure M-5 shows the axial mass flux of water vapor in the gas phase along the central drift in the model, plotted for the upstream end of each of the four waste packages (the end closer to the repository center), and also at the repository edge (the downstream end of the last waste package). Note that Figure M-1 shows the waste package sequence. These results were calculated using the most realistic D/LMTH case, as noted. The curves are parallel, with the upstream value being less than the downstream value at a given waste package location, with the exception of the two curves labeled PWR1 (the outermost waste package) and Repository Edge, which drop below the value of the respective upstream curves at approximately 300 years and signify that condensation is occurring in the vicinity of the cooler DOE high-level radioactive waste package after approximately 300 years.

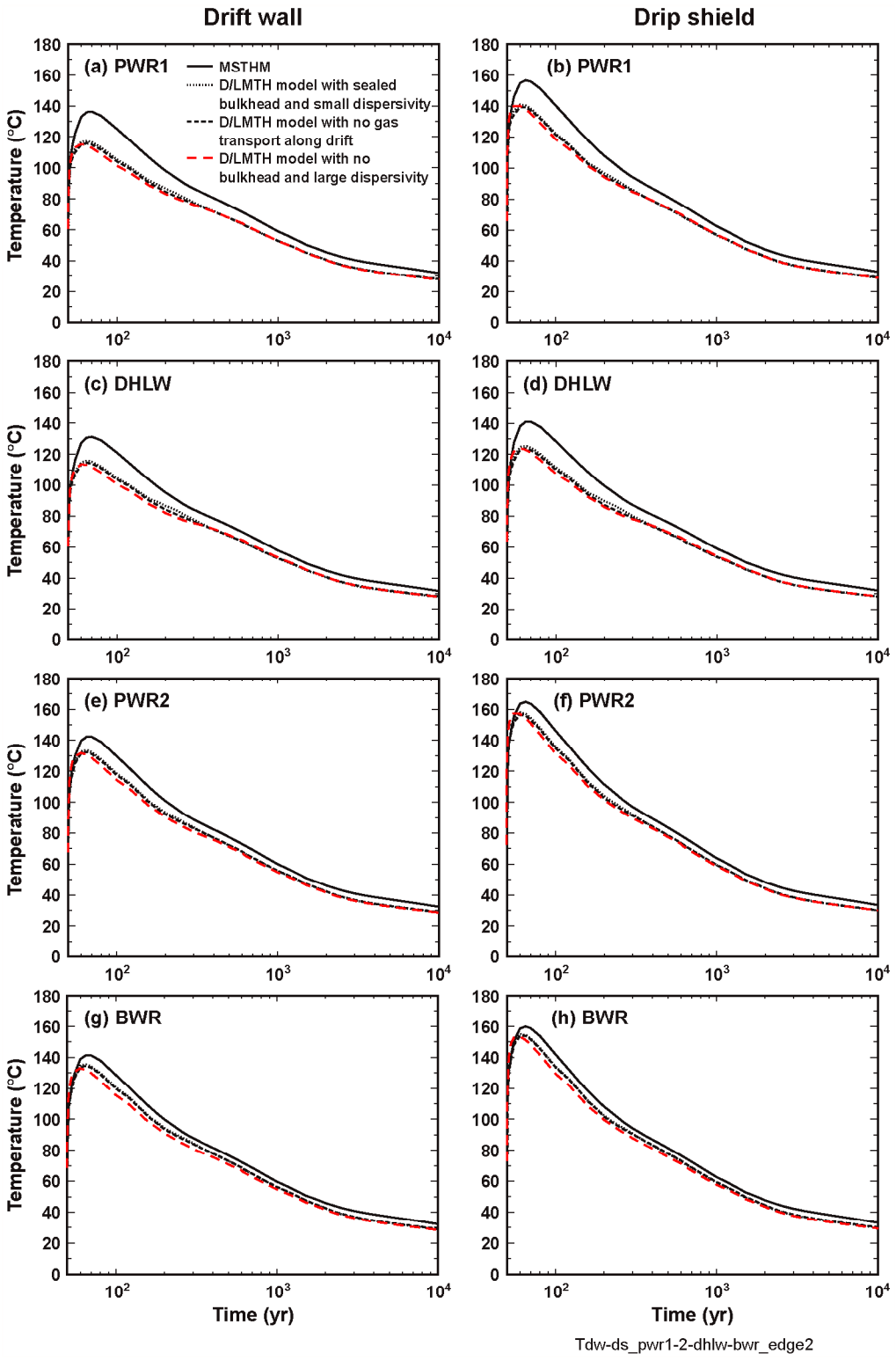

Source: BSC 2004b, Figure 7.5-5; DTN: LL040703223122.050.

Figure M-2. Drift-Wall and Drip-Shield Temperature Versus Time for the (a, b) PWR1, (c, d) DOE High-Level Radioactive Waste, (e, f) PWR2, and (g, h) BWR Waste Packages at the Edge of the Three-Drift Repository

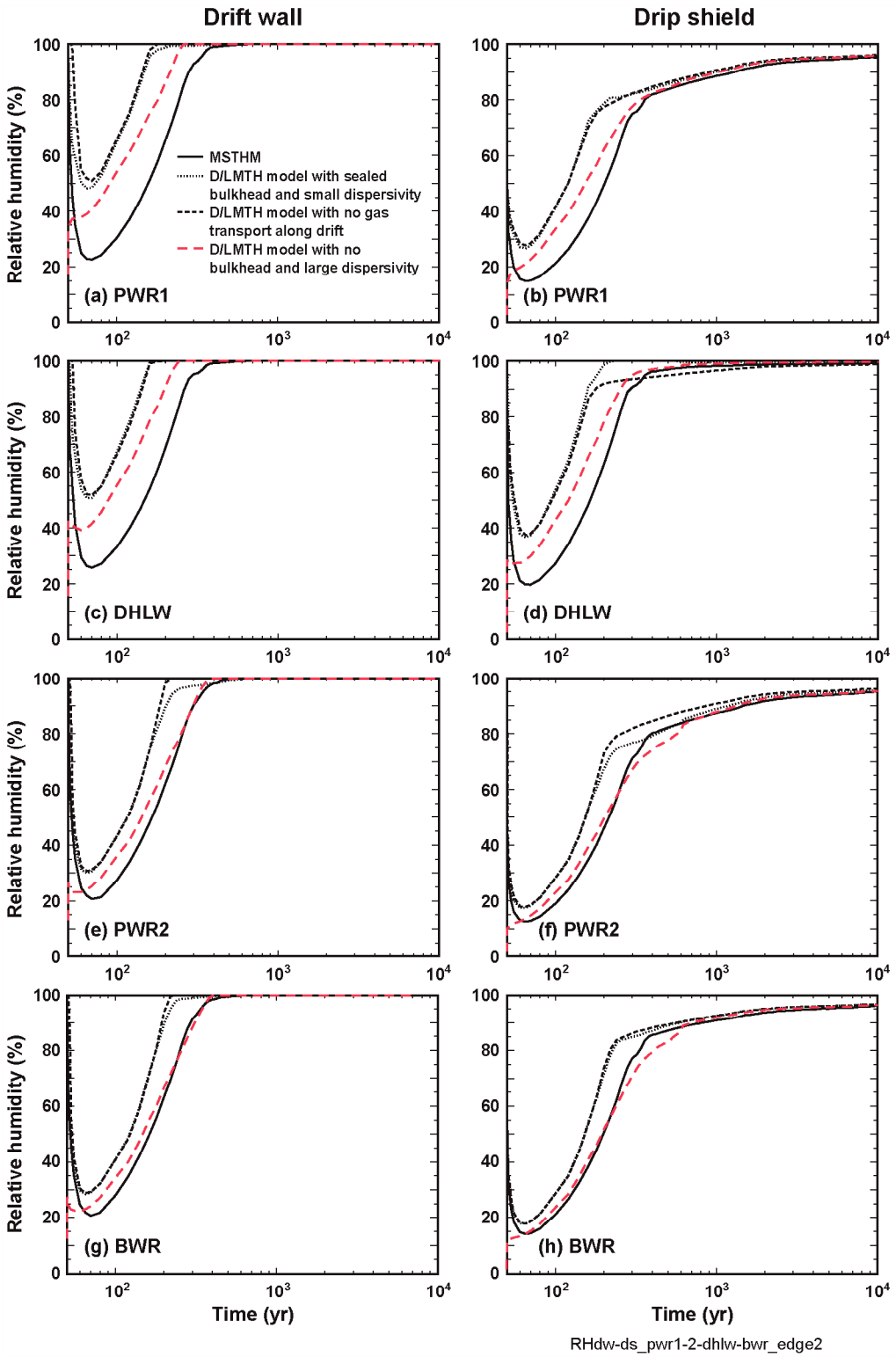

Source: BSC 2004b, Figure 7.5-6; DTN: LL040703223122.050.

Figure M-3. Drift-Wall and Drip-Shield Relative Humidity Versus Time for the (a, b) PWR1, (c, d) DOE High-Level Radioactive Waste, (e, f) PWR2, and (g, h) BWR Waste Packages at the Edge of the Three-Drift Repository

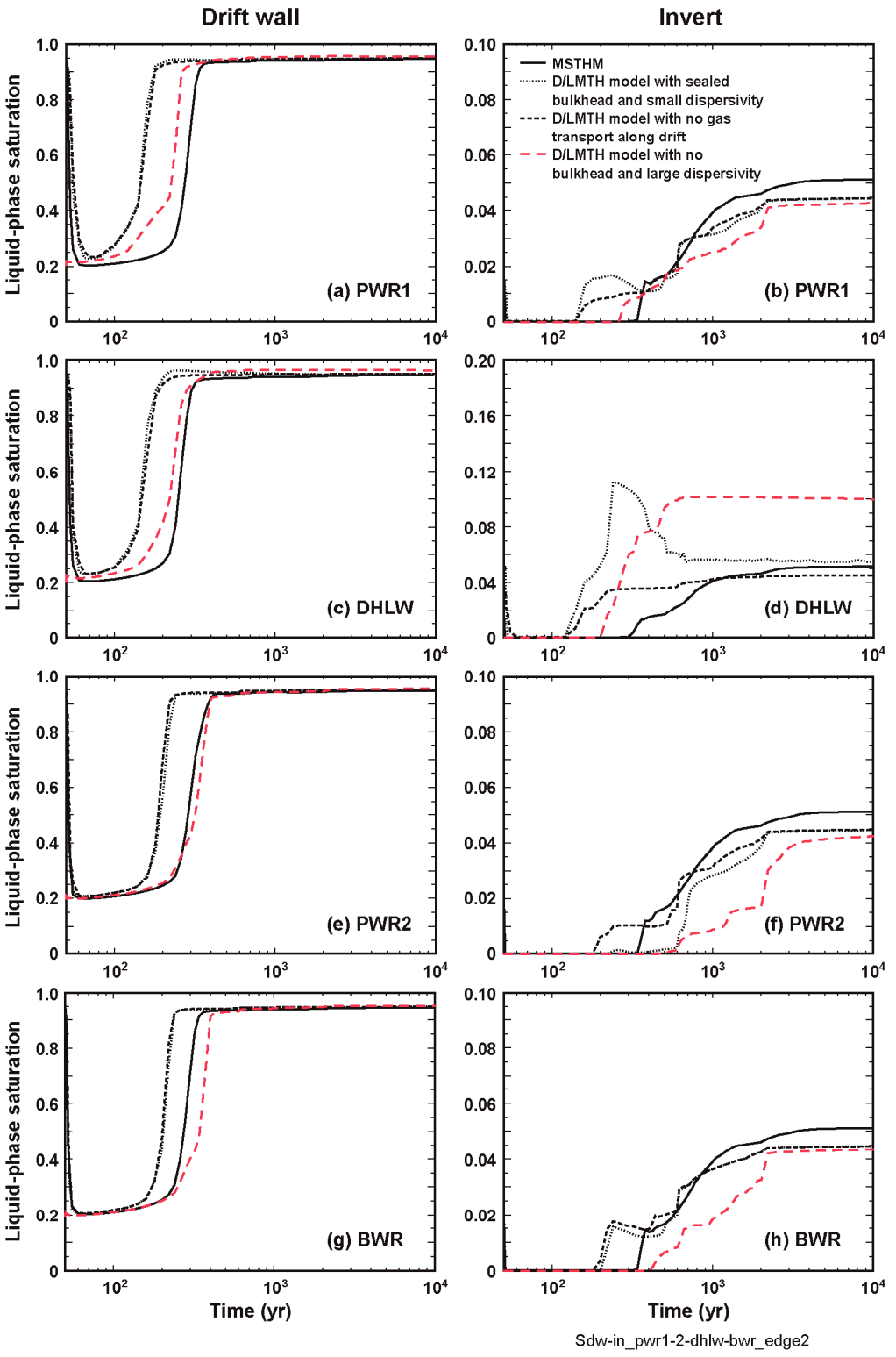

Source: BSC 2004b, Figure 7.5-7, DTN: LL040703223122.050.

Figure M-4. Drift-Wall and Invert Liquid-Phase Saturation Versus Time for the (a, b) PWR1, (c, d) DOE High-Level Radioactive Waste, (e, f) PWR2, and (g, h) BWR Waste Packages at the Edge of the Three-Drift Repository

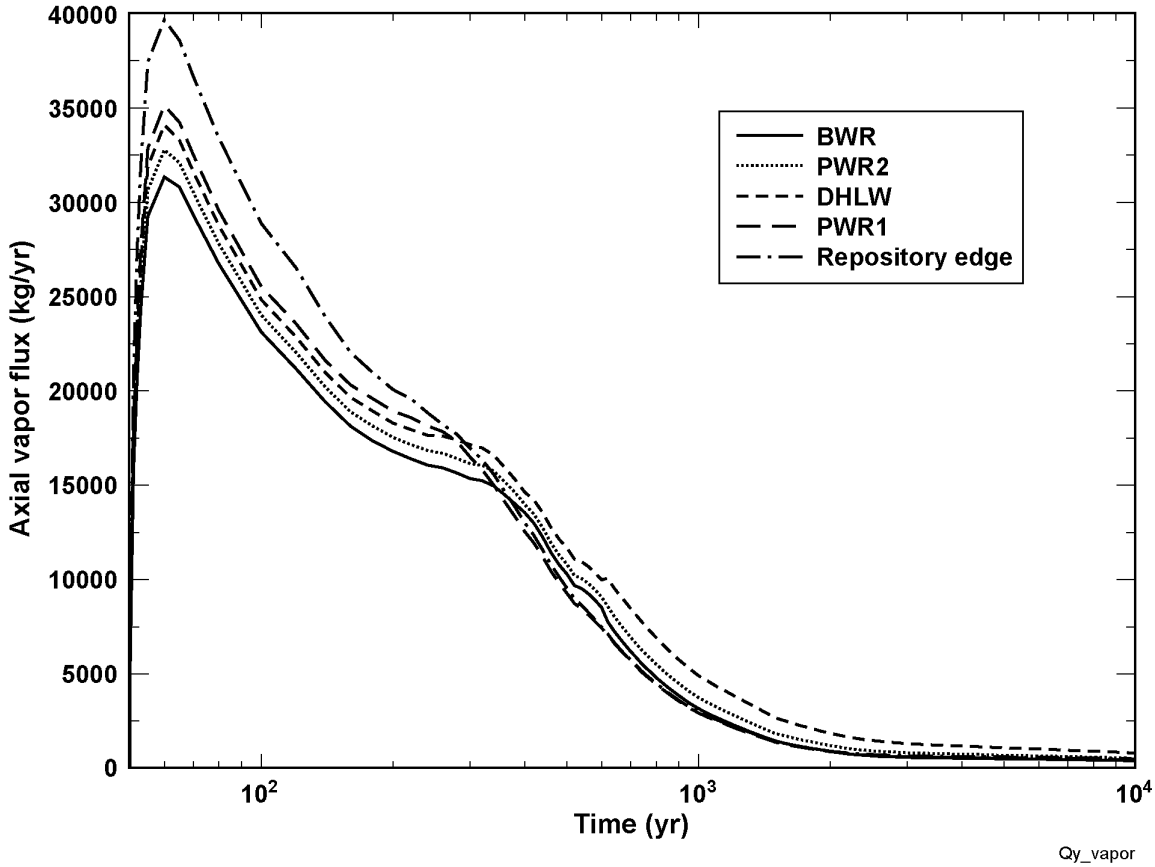

Source: DTN: LL040703223122.050.

NOTE: This figure corresponds to the D/LMTH-model case with gas transport along drift with a high gas-phase dispersion coefficient (case 3). This case also includes the influence of host-rock dryout during the ventilation period. The waste package sequencing, starting from the edge, is PWR1, DHLW, PWR2, and BWR, as is shown in Figure M-1. The upstream side of the waste package is the side closer to the repository center. The repository edge curve corresponds to the downstream side of the PWR1 waste package. The PWR1 curve corresponds to the upstream side of the PWR 1 waste package and to the downstream side of the DHLW waste package. The DHLW curve corresponds to the upstream side of the DHLW waste package and to the downstream side of the PWR2 waste package. The PWR2 curve corresponds to the upstream side of the PWR2 waste package and to the downstream side of the BWR waste package. The BWR curve corresponds to the upstream side of the BWR waste package.

Figure M-5. Axial Vapor Flux on the Upstream Side of the Listed Waste Packages at the Edge of the Three-Drift Repository

Tables M-1 to M-4 show moisture balance results for each of the four outermost waste packages at the repository edge, from the D/LMTH model case with no bulkhead and large dispersivity (case 3). The phase change columns show where evaporation (positive values) and condensation (negative values) are occurring at each waste package location for several discrete times distributed over the regulatory period. Note that the delta axial vapor flux, which is the difference in axial vapor flux between the upstream and downstream sides of a waste package (see Figure M-5), corresponds to the net condensation or evaporation occurring at a waste package location. The radial vapor flux corresponds to the phase change that occurs in the host rock. Thus, the sum of the radial vapor flux, the invert phase change, and the drift phase change is equal to the delta axial vapor flux. Of the four waste packages, the DOE high-level radioactive waste package (Table M-2) is the coolest, and condensation occurs mainly there. A comparison of the delta axial vapor flux with the radial vapor flux shows that most of the condensation at the cooler waste package results from water vapor migration outward into cooler rock, where it condenses. This water is then diverted around the drift opening along with the ambient percolation flux.

Tables M-1 to M-4 and Figures M-3 to M-5 show that evaporation from the drift wall prevails even at the edge of the repository, which cools earlier than repository center locations. The model shows that condensation is strongest in the unheated part of the drift, particularly during the early stage of repository thermal evolution when repository center temperatures are greater than boiling (96°C). The region of the repository layout area in which condensation occurs on cooler waste packages moves inward from the edge, starting after approximately 300 years of cooling.

Table M-1. Summary of Moisture Balance for PWR1 Waste Package in Multiscale Thermal-Hydrologic Model Validation Test Case

Time (years)	Vapor Flux (kg/yr)				Phase Change (kg/yr)	
	Axial (upstream)	Axial (downstream)	Delta Axial	Radial	Invert	Drift
60	35,137.6	39,680.5	4,542.9	4,300.3	242.8	0.0
100	25,530.0	28,876.8	3,346.8	3,113.4	233.3	0.0
500	9,273.2	9,554.1	280.9	51.9	229.5	−0.4
1,000	2,928.7	2,978.4	49.7	−59.4	109.1	0.0
2,000	878.3	904.4	26.1	−17.6	51.6	−7.9
5,000	547.5	603.6	56.1	19.3	36.8	0.0
10,000	448.7	499.4	50.7	21.5	29.1	0.0

Source: DTN: LL040703223122.050.

NOTE: The PWR1 waste package is located at the outer edge of the three-drift validation test case (BSC 2004b, Figure 7.5-1) for the D/LMTH model with no bulkhead and a high gas-phase dispersion coefficient along the drift. Positive values of radial vapor flux correspond to vapor leaving the host rock and entering the drift (and invert); negative values correspond to vapor leaving the drift (and invert) and entering the host rock. Positive values of phase change correspond to evaporation; negative values correspond to condensation. The delta axial vapor flux, which is the difference in axial vapor flux between the upstream and downstream sides of a waste package (see Figure M-5), corresponds to the net condensation or evaporation occurring at a waste package location. The radial vapor flux corresponds to the phase change that occurs in the host rock. Thus, the sum of the radial vapor flux, the invert phase change, and the drift phase change is equal to the delta axial vapor flux.

Table M-2. Summary of Moisture Balance for DOE High-Level Radioactive Waste Package in Multiscale Thermal-Hydrologic Model Validation Test Case

Time (years)	Vapor Flux (kg/yr)				Phase Change (kg/yr)	
	Axial (upstream)	Axial (downstream)	Delta Axial	Radial	Invert	Drift
60	34,102.0	35,138.0	1,036.0	1,036.0	0.0	0.0
100	24,835.0	25,530.0	695.0	695.0	0.0	0.0
500	11,679.4	9,273.2	−2,406.2	−2,381.4	−12.5	−12.4
1,000	4,902.1	2,928.7	−1,973.4	−1,920.2	−30.4	−22.8
2,000	1,851.1	878.3	−972.8	−925.7	−19.1	−28.0
5,000	1,076.4	547.5	−528.8	−495.0	−10.4	−23.4
10,000	800.6	448.7	−351.9	−332.2	−6.6	−13.1

Source: DTN: LL040703223122.050.

NOTE: The DOE high-level radioactive waste package is the second to the last waste package located at the outer edge of the three-drift validation test case (BSC 2004b, Figure 7.5-1) for the D/LMTH model with no bulkhead and a high gas-phase dispersion coefficient along the drift. Positive values of radial vapor flux correspond to vapor leaving the host rock and entering the drift (and invert); negative values correspond to vapor leaving the drift (and invert) and entering the host rock. Positive values of phase change correspond to evaporation; negative values correspond to condensation. The delta axial vapor flux, which is the difference in axial vapor flux between the upstream and downstream sides of a waste package (see Figure M-5), corresponds to the net condensation or evaporation occurring at a waste package location. The radial vapor flux corresponds to the phase change that occurs in the host rock. Thus, the sum of the radial vapor flux, the invert phase change, and the drift phase change is equal to the delta axial vapor flux.

Table M-3. Summary of Moisture Balance for PWR2 Waste Package in Multiscale Thermal-Hydrologic Model Validation Test Case

Time (years)	Vapor Flux (kg/yr)				Phase Change (kg/yr)	
	Axial (upstream)	Axial (downstream)	Delta Axial	Radial	Invert	Drift
60	32,775.4	34,102.0	1,326.6	1,326.9	0.0	0.0
100	24,014.0	24,835.0	821.0	821.0	0.0	0.0
500	10,813.1	11,679.4	866.3	711.8	153.7	0.8
1,000	3,744.8	4,902.1	1,157.3	1,062.5	94.8	0.0
2,000	1,202.0	1,851.1	649.1	592.5	56.6	0.0
5,000	678.6	1,076.4	397.8	348.9	48.8	0.0
10,000	524.7	800.6	275.9	238.2	37.7	0.0

Source: DTN: LL040703223122.050.

NOTE: The PWR2 waste package is the third to the last waste package located at the outer edge of the three-drift validation test case (BSC 2004b, Figure 7.5-1) for the D/LMTH model with no bulkhead and a high gas-phase dispersion coefficient along the drift. Positive values of radial vapor flux correspond to vapor leaving the host rock and entering the drift (and invert); negative values correspond to vapor leaving the drift (and invert) and entering the host rock. Positive values of phase change correspond to evaporation; negative values correspond to condensation. The delta axial vapor flux, which is the difference in axial vapor flux between the upstream and downstream sides of a waste package (see Figure M-5), corresponds to the net condensation or evaporation occurring at a waste package location. The radial vapor flux corresponds to the phase change that occurs in the host rock. Thus, the sum of the radial vapor flux, the invert phase change, and the drift phase change is equal to the delta axial vapor flux.

Table M-4. Summary of Moisture Balance for BWR Waste Package in Multiscale Thermal-Hydrologic Model Validation Test Case

Time (years)	Vapor Flux (kg/yr)				Phase Change (kg/yr)	
	Axial (upstream)	Axial (downstream)	Delta Axial	Radial	Invert	Drift
60	31,340.2	32,775.4	1,435.2	1,435.3	0.0	0.0
100	23,118.2	24,014.0	895.8	895.7	0.0	0.0
500	10,292.6	10,813.1	520.5	389.3	130.2	1.0
1,000	3,161.5	3,744.8	583.3	500.9	82.4	0.0
2,000	889.2	1,202.0	312.8	264.5	48.4	0.0
5,000	489.6	678.6	189.0	155.7	33.4	−0.1
10,000	400.8	524.7	123.9	98.7	26.3	−1.1

Source: DTN: LL040703223122.050.

NOTE: The BWR waste package is the fourth to the last waste package located at the outer edge of the three-drift validation test case (BSC 2004b, Figure 7.5-1) for the D/LMTH model with no bulkhead and a high gas-phase dispersion coefficient along the drift. Positive values of radial vapor flux correspond to vapor leaving the host rock and entering the drift (and invert); negative values correspond to vapor leaving the drift (and invert) and entering the host rock. Positive values of phase change correspond to evaporation; negative values correspond to condensation. The delta axial vapor flux, which is the difference in axial vapor flux between the upstream and downstream sides of a waste package (see Figure M-5), corresponds to the net condensation or evaporation occurring at a waste package location. The radial vapor flux corresponds to the phase change that occurs in the host rock. Thus, the sum of the radial vapor flux, the invert phase change, and the drift phase change is equal to the delta axial vapor flux.

Thermal-Hydrologic Conditions in the Invert–The three-drift D/LMTH model described above (case 3) was used to investigate where condensation might occur in the drifts and the conditions in the invert that could contribute to condensation under the drip shield. Model results (Table M-2) predict that the majority of the condensation in the vicinity of the cold DOE high-level radioactive waste package near the repository edge occurs in the host rock with relatively little condensation in the invert or at the drift wall. Only a small percentage of the total condensation at this waste package occurs in the invert. Evaporation rates in the invert below the two hotter waste packages (PWR1 and PWR2) on either side (Invert Phase Change in Tables M-1 and M-3) are also small compared to the evaporation rates occurring in the adjoining host rock. It is important to note that the majority of the water vapor that has the potential of condensing on the underside of the drip shield would originate from the invert (particularly, the upper portion of the invert), where it would have evaporated. Therefore, relatively small magnitudes of evaporation and condensation fluxes in the invert are indicative of small potential condensate fluxes on the underside of the drip shield. These results indicate that the preponderance of axial vapor flow along the drift occurs outside the drip shield; consequently, the magnitude of condensation on the underside of a drip shield, if it occurs, is very small compared to the total condensation at any waste package location. Similarly, the magnitude of the condensate flux in the invert is small compared to the total condensation flux at any waste package location. The findings are based on the drip shield and waste package being lumped into one monolithic unit, thus ignoring the effect of the air space underneath the drip shield on vapor transport along the drift axis. This modeling assumption limits the applicability of the results; however, these analyses provide an alternative means to assess vapor flow and transport in the drift. The calculated maximum difference between drift-wall temperatures at adjacent waste package locations is approximately 25 C° (BSC 2004b, Figures 7.5-2 and 7.5-5). The

temperature effect is included in the *Multiscale Thermohydrologic Model* (BSC 2004b) results used for the TSPA-LA (BSC 2004b, Section 6.3).

Process Model Results Summary–The emplacement drift opening exerts minimal resistance to gas flow, serving as a preferential conduit for water vapor. Boiling of water in the host rock causes the gas-phase pressure to rise locally, which drives water vapor to the unheated parts of the drifts where it condenses, lowering the pressure locally. Because of the minimal resistance to gas-phase flow in the drift air, and because the heated parts of the drifts communicate freely with the unheated openings, gas-phase pressure buildup in the emplacement drift is small. (The pressure rise is on the order of a few Pascals; the precise magnitude is uncertain from the output of the porous-medium model but is not needed to conclude that resistance to flow is minimal.)

Much of the water vapor generated by boiling in the host rock flows radially into the emplacement drift and then axially toward the repository edge. Thermally driven convective mixing augments the transport of vapor in the axial direction, represented by the gas-phase dispersion coefficient in the model. When the entire heated portion of the drift is above the boiling point, the transported water vapor in the drift reaches the unheated portion of the drift beyond the last waste package, where it condenses. After the drift wall adjacent to the coolest waste package near the edge (the DOE high-level radioactive waste package in Table M-2 and Figure M-5) cools below boiling (96°C), some of this transported water vapor condenses in the vicinity of the cold waste package. As repository cooling proceeds, condensation occurs on other, cooler waste packages farther from the edge.

Screening of Cold-Trap Effects in the Rock above Cooler Waste Packages–Temperature, relative humidity, and liquid-phase saturation predicted by the multiscale thermal-hydrologic model are in good agreement with those predicted by the D/LMTH model that includes the cold-trap effect (case 3) and the influence of rock dryout during the ventilation period. Although the multiscale thermal-hydrologic model does not directly account for the influences of the cold-trap effect or of rock dryout during the ventilation period, it does compare well with the alternative model that includes both of these influences. Therefore, it is unnecessary to incorporate the host-rock cold-trap effect into the multiscale thermal-hydrologic model, justifying its exclusion from the multiscale thermal-hydrologic model calculations that support the TSPA-LA. Inclusion of the effects of increased flux due to condensation on drift walls has been addressed in TSPA through implementation of results of the network model described in the following section.

M.4.2 In-Drift Condensation (Network) Model, Results, and Discussion

The evaluation of vapor transport in the drifts uses two types of models. The first type is described in Section M.4.1. This section describes the second type: a one-dimensional, lumped parameter model, or network model, of the in-drift components. This network model is described in *In-Drift Natural Convection and Condensation Model* (BSC 2003a). This section summarizes the model and those aspects pertinent to the cold-trap effect.

The coolest temperatures at a particular waste package location are generally found at the drift wall, particularly the drift wall beneath the invert (BSC 2003a, Section 6.3.3). Considering multiple waste package locations, the drip shield over a cooler waste package may be cooler than the drift wall at the location of a hotter waste package. Vapor transport and condensation will

likely be driven by temperature differences over a distance less than the drift diameter or a greater distance corresponding to two or more waste packages. These effects are referred to in the following discussion as the waste package scale or drift-scale of condensation behavior.

At the end of each emplacement drift, part of the drift contains no waste packages and is, therefore, unheated. On the inner end (closer to the repository center) is the exhaust standoff and exhaust drift. On the outer end is the access turnout and access drifts. Both of these drift sections are substantially cooler than the heated part. Vapor from the heated region will migrate to these cooler zones and condense. This is the repository scale.

Early during thermal evolution of the repository, the drive for movement of water vapor in the drifts includes overpressure produced by water boiling from the host rock. After several hundred years of cooling, that drive will be less important, and gas-phase transport within the emplacement drifts is controlled by drift-scale natural convection, repository-scale natural convection and natural ventilation, and barometric pumping. Drift-scale natural convection generates axial and radial convection cells in the drifts in response to differences in the temperature of the waste packages, drip shields, and the host rock. Repository-scale natural convection and natural ventilation can result from temperature differences between the emplacement drifts, the other connected openings, and the host rock. Barometric pumping is driven by atmospheric pressure fluctuations that drive air into or out of the unsaturated zone and push air into and out of the emplacement drifts. For the condensation network model, estimation of dispersive transport in the drifts is limited to the drift-scale convective processes. Barometric pumping and repository-scale natural convection and natural ventilation are acknowledged as processes that would further enhance the axial transport of water vapor (BSC 2003a, Section 6.3.7.3).

In principle, the details of evaporation and condensation processes in the emplacement drifts could be modeled in a computational fluid dynamic code like FLUENT (Fluent 2001). As a practical matter, the dimensions of the typical problem are computationally intractable. For this reason, the condensation network model incorporates a one-dimensional axial dispersion approach to represent evaporation, transport, and condensation of water vapor. In this approach, the axial transport is characterized by an axial dispersion coefficient for the gas outside the drip shield and a dispersion coefficient for the region under the drip shield. (The same dispersion coefficient is used in the three-dimensional porous-medium model described previously.)

The condensation network model represents every waste package in an emplacement drift, as well as locations within the unheated parts of the drift using a lumped-parameter approach. The model is parameterized to represent each of seven representative emplacement drifts chosen to span the range of behavior throughout the repository (Figure M-6). Line-source thermal conduction solutions are used to approximate the drift-wall temperature based on the actual repository layout. Temperatures for the waste package, drip shield, and invert surface are calculated for each waste package location. Local evaporation and condensation rates are computed using standard heat and mass transfer correlations based on temperatures and vapor mass fractions. The vapor fraction of the gas is calculated as a function of axial position along the drift (BSC 2003a, Section 6.3.7.2).

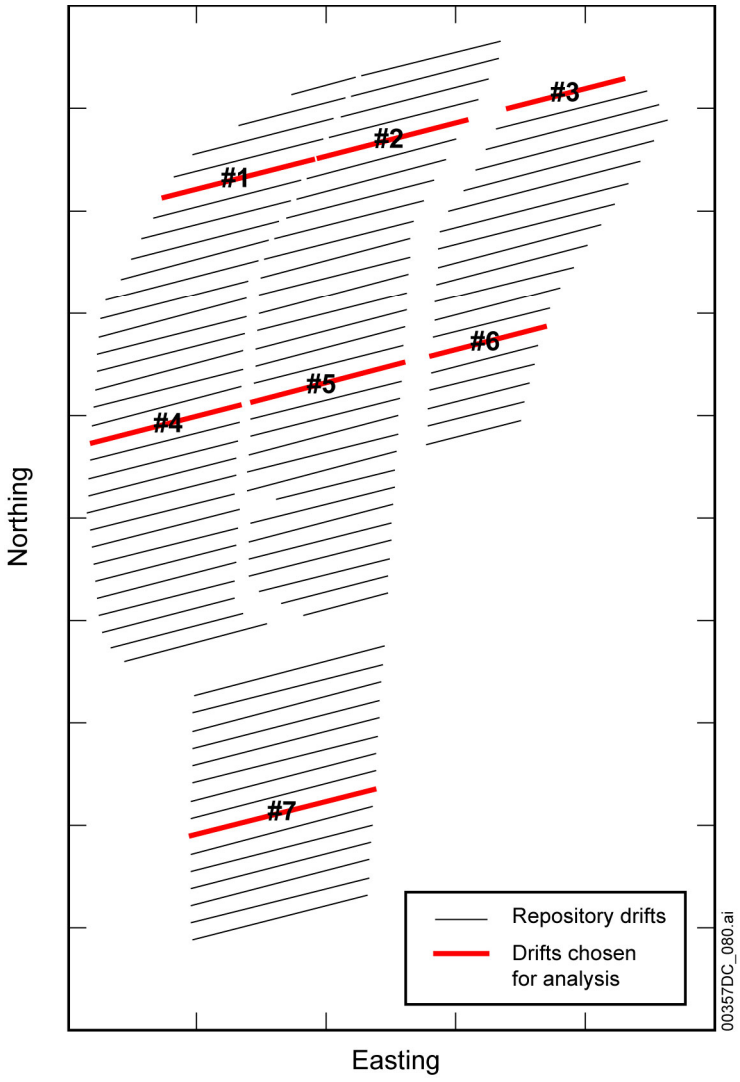

Source: BSC 2003a, Figure 6.3.7-1.

Figure M-6. Repository Drifts Chosen for Analysis

The axial dispersion coefficient is estimated from drift-scale FLUENT computational fluid dynamic calculations for a unit-cell arrangement in the emplacement drift containing the same repeated pattern of hot and cold waste packages that is used for the multiscale thermal-hydrologic model. The FLUENT computational fluid dynamic case consists of a 71-m length of drift containing 14 waste packages. Individual waste packages are modeled, including the drip shield and invert, as well as 5 m of rock surrounding the drift. The individual waste package heat outputs are used, and natural convection and thermal radiation are calculated based on the Navier-Stokes equations, including turbulence. The resulting natural convection flow pattern consists of hot and cold waste packages pairing off, local convection cells, and larger convection cells within the 71-m drift. The flow patterns are a strong function of the temperature gradient in the host rock surrounding the drift (BSC 2003a, Section 6.2.7).

Once these convection cells are calculated by the FLUENT code, values for the dispersion coefficient to be used in the condensation network model are evaluated using a neutrally buoyant trace gas species. A lower bound for the dispersion coefficient is calculated by ignoring the effect of the axial temperature gradient on the flow in the unit cell. A higher value for the dispersion coefficient is calculated by applying an axial temperature gradient to the unit cell. These two values provide reasonable bounds for the uncertainty of the axial dispersion coefficient in the condensation network model (BSC 2003a, Section 6.2.7).

The drift wall constitutes the source of water vapor for the condensation network model. The amount of water that can be evaporated from the drift wall and invert surfaces is limited by the supply of water in the surrounding rock. Since the model does not include coupling to the host rock, an estimate of the supply of water vapor is calculated from the bounds on capillary pumping through the rock matrix and the percolation flux. Fracture percolation predominates. The uncertainty on infiltration is incorporated through the use of the corresponding lower, mean, and upper percolation flux estimates averaged over the length of each drift evaluated. These percolation values change at the project step changes in climate (600 and 2,000 years after closure). This approach is bounding and different from the porous-medium model, which incorporates multiphase flow processes, rock dryout, and other features that tend to limit the production of water vapor into the drift opening (BSC 2003a, Section 6.3.7.2.4). The vapor mass fraction boundary conditions at all surfaces (drift wall, invert, drip shield, and waste packages) are computed by applying saturation conditions for the local surface temperature. At the temperatures of interest, small differences in temperature (on the order of 1 C° to 5 C°) correlate to notable differences in evaporation magnitudes, as discussed below. The network model represents the invert as a single component, such that its temperature is uniform from the top to the bottom at the interface between the invert and host rock as compared to the porous-medium approach in which the invert is modeled as a three-dimensional entity.

The possibility and location of invert evaporation are important to evaluation of potential condensation under the drip shields. The invert surface under hotter waste packages is typically hotter than the drip shield surface associated with cooler waste packages at nearby locations. Thus, if evaporation occurs at the top of the invert, where its temperature is greatest, then condensation under a nearby drip shield is possible. However, if evaporation occurs at the bottom of the invert, where it is cooler, the network model results show that condensation does not occur under the drip shield at any location. Evaporation at the top of the invert will be governed by temperature and the mass fraction of water present in invert particles and fractures (BSC 2004a, Section 6.2.41). In the multiscale thermal-hydrologic model results discussed previously, seepage is not included, and the top of the invert remains relatively dry (BSC 2004b). The condensation network model includes two limiting cases representing uncertainty in the source condition for partial pressure of water vapor in the invert: the high- and low-invert transport cases corresponding respectively to evaporation at the top and bottom of the invert (BSC 2003a, Section 6.3.7.3).

The drip shield design allows gas flow through the joints where the segments overlap. In addition, gas flow through the invert ballast material allows additional mass exchange between the gas phase underneath the drip shield and that outside the drip shield. Model results show that condensation under the drip shield does not occur if this gas exchange is sufficiently great. To represent uncertainty in the potential for gas exchange, model cases were generated using

equalized gas-phase composition across the drip shield and unequalized conditions that maximize the difference in composition (BSC 2003a).

Condensation is only possible when the surfaces inside the emplacement region lie below the ambient saturation temperature. At the height of the thermal period, the entire emplacement region will be above the saturation temperature. At later times, the entire emplacement region will be below the saturation temperature. The current condensation model addresses only this later time period. The intermediate period, in which portions of the emplacement region lie above and below the saturation region, is not explicitly represented by the model. However, the intermediate period was evaluated using the porous-medium model described previously, and the condensation behavior is similar, starting gradually as cooler waste packages cool below boiling (96°C). On this basis, the condensation network model is applied for the intermediate period, which typically lasts from approximately 300 to 700 years.

The seven emplacement segments are shown in the repository layout (Figure M-6). Segments 1 to 3 are colinear and lie near the northern edge of the repository. Edge effects of three-dimensional conduction are pronounced there. Segments 4 to 6 are colinear and are in the middle of the repository where temperatures are generally greatest. Segment 7 is in the southern lobe of the repository where the drift lengths are longest. All seven drifts were analyzed at times of 1,000, 3,000, and 10,000 years. Drift segment 3 was also analyzed at 300 years because it cools faster than the other six drifts.

Figure M-7 presents calculated condensation on the drift wall for the limiting case of a completely ventilated drip shield and a low-invert transport assumption. The top portion of Figure M-7 shows the vapor mass fraction in the gas (red dashed line) and the equilibrium vapor mass fraction for the drift wall based upon the drift-wall temperature (solid blue line). In the center of the drift, the axial transport causes the gas vapor pressure to be lower than the equilibrium vapor pressure at the drift wall where water is evaporating.

Progressing from the drift center, the gas vapor pressure reaches a point where it is slightly higher than the equilibrium vapor pressure at the drift wall. The scaling of this figure obscures the very small differences that exist in this region. However, the lower plot in Figure M-7 clearly depicts this difference in the occurrence of condensation. A portion of the axially transported water vapor condenses on the drift wall in these two regions near the edges of the emplacement drifts. The rate of condensation on the drift wall in these regions is determined by the vapor mass fraction difference between the gas and the wall and the thickness of the gas boundary layer.

In the regions between the two condensation zones and the nonemplacement portions of the drift (i.e., the access turnout and the exhaust standoff, indicated by the vertical dashed lines), the vapor mass fraction in the gas again dips below the equilibrium mass fraction at the wall. As in the center of the drift, water evaporates from the drift wall in these two regions. This evaporated water combines with the axially transported water vapor that made it through the condensation zones and condenses in the unheated parts of the drift. Figures M-7 to M-9 do not include condensation in these regions (although it is predicted to occur) in order to highlight condensation on the emplacement drift walls.

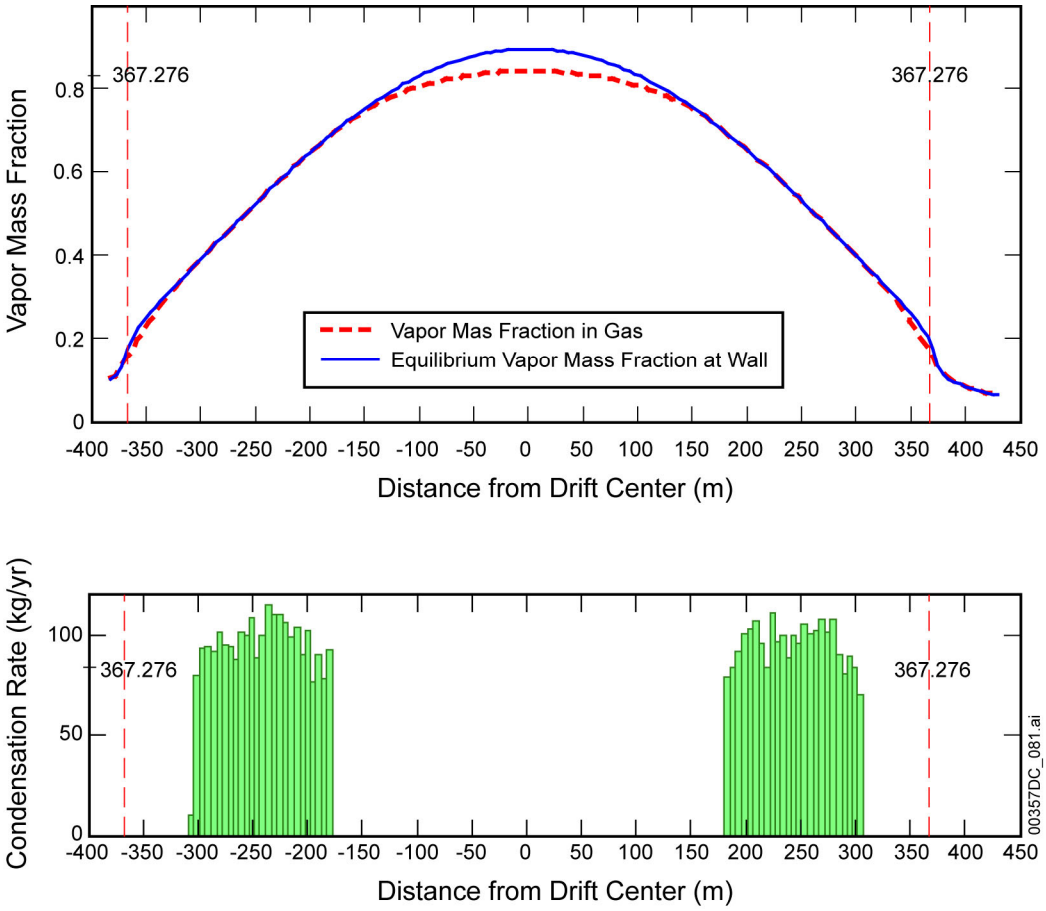

Source: BSC 2003a, Figure 6.3.7-2.

Figure M-7. Representative Vapor Mass Fraction in Gas (Top) and Condensation Rate per Waste Package on Drift Wall (Bottom): Segment 7, 1,000-year, Mean Percolation Rate, Well-Ventilated Drip Shield, Low Invert Transport, Low-Dispersion Coefficient as a Function of Distance from the Center of the Drift

Figure M-8 addresses condensation on the drift wall for a second case of a well-ventilated drip shield and assuming a high-transport invert. Comparison of these results to the limiting case presented in Figure M-7 reveals the sensitivity of the model to assumptions regarding invert behavior. Figure M-8 shows the location and magnitude of condensation on the drift wall at 1,000 years for the mean percolation case. Condensation rates on the drift walls for the high-transport invert are about twice those depicted in Figure M-7.

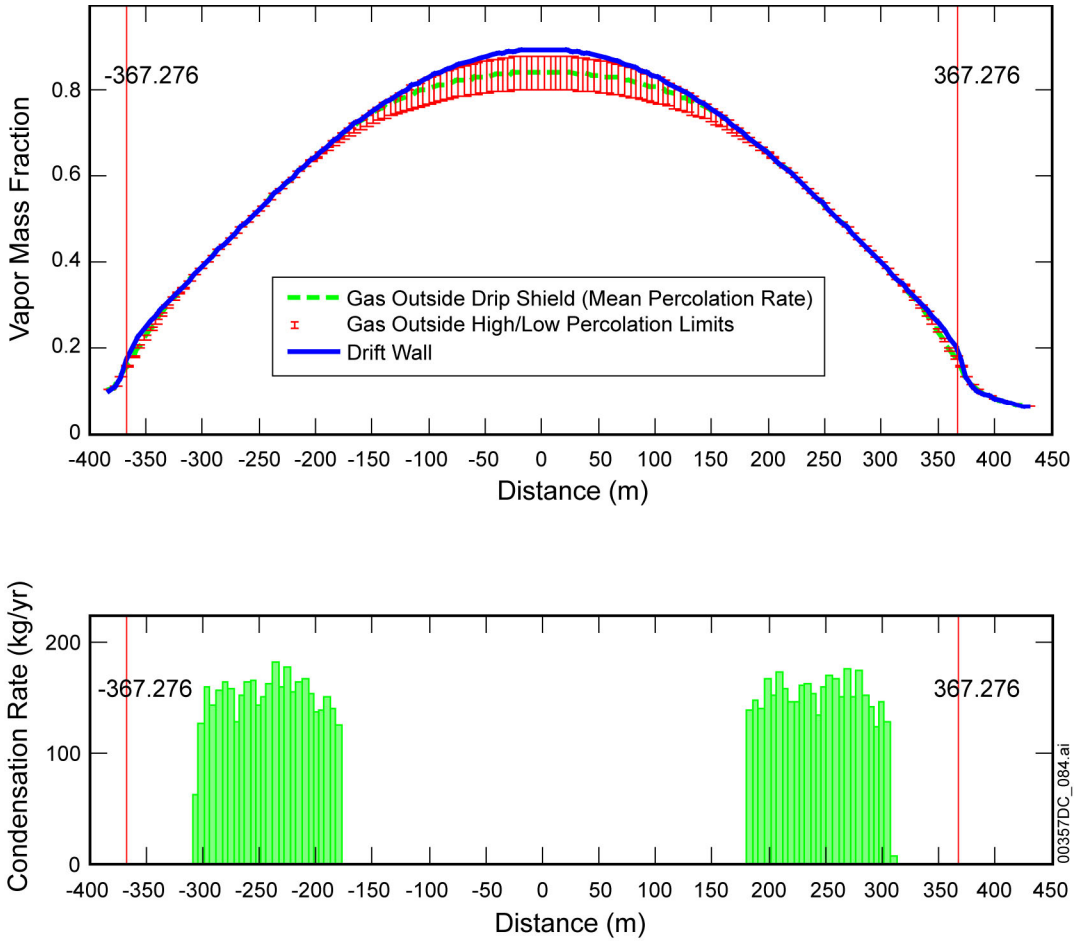

Source: BSC 2003a, Figures E.2-1 and E.2-2.

Figure M-8. Representative Vapor Mass Fraction in Gas (Top) and Condensation Rate per Waste Package on Drift Wall (Bottom): Segment 7, 1,000-year, Mean Percolation Rate, Well-Ventilated Drip Shield, High Invert Transport, Low-Dispersion Coefficient as a Function of Distance from the Center of the Drift

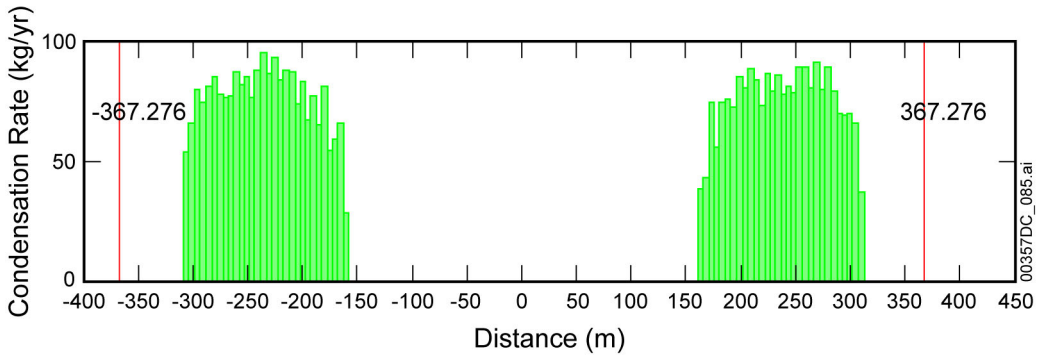

Source: BSC 2003a, Figure E.4-2.

Figure M-9. Representative Condensation Rate per Waste Package on Drift Wall: Segment 7, 1,000-year, Mean Percolation Rate, Poorly Ventilated Drip Shield, High Invert Transport, Low-Dispersion Coefficient as a Function of Distance from the Center of the Drift

Additional cases were also executed for the network model implementing a poorly ventilated drip shield. Predictions for the high-transport, unventilated drip shield case indicate that there is a possibility of condensation on the underside of the drip shield for this set of assumptions. However, as discussed below, this case is screened out of TSPA-LA on the basis of low consequence. The following trends are obtained from the condensation analysis (BSC 2003a, Section 6.3.7.2 and Attachment E):

- Greater axial dispersion transports more of the evaporated water to the unheated parts of the drifts, decreasing condensation in the emplacement region.

- The rate of condensation in the emplacement region may increase with time because of smaller temperature differences across the length of the drifts, as well as increased percolation rates. Evaporation and condensation are limited by availability of water and not by the available thermal power.

- Invert evaporation and the gas-phase mass exchange across the drip shield affect the probability and quantity of condensation under the drip shield.

The condensation network model provides four cases for a low axial dispersion coefficient and four cases for a high axial dispersion coefficient. Model results from the high and low limiting cases of invert transport shown in Figures M-7 and M-8 capture the range of probable occurrence and rates of condensation within the drift environment for a well-ventilated drip shield. These results are considered appropriate because:

- The axial dispersion coefficients developed from computational fluid dynamic calculations include only barometric pumping effects and drift-scale convective effects and not the repository-scale natural convection and natural ventilation. Inclusion of these effects in the estimates for axial dispersion coefficients would increase transport with a probable concomitant decrease in predicted condensation in the emplacement regions. Results (not shown, but presented in *In-Drift Natural Convection and Condensation Model* (BSC 2003a)) using a high axial dispersion coefficient predict much lower rates of condensation. Hence, the cases shown in this document provide a reasonable upper bound on drift wall condensation for a well-ventilated drip shield configuration.

- Invert evaporation rates are expected to be lower than those predicted by the high-transport invert case if water flow in the invert is examined more closely. As discussed below and in *Multiscale Thermohydrologic Model* (BSC 2004b, Section 7.5), significantly lower invert evaporation and condensation rates are predicted using the three-dimensional three-drift porous-medium model.

- Mixing of the gases beneath the drip shield and the region between the drip shield and drift wall relies on uncertainties in invert and drip shield construction parameters. The primary impact of condensation within the in-drift environment will be to enhance advective fluxes from the drift to the unsaturated zone. The cases presented in Figures M-7 and M-8 provide reasonable bounds on the possible increase in water (and, consequently, radionuclide) flux from the in-drift environment. This represents a

reasonable approximation when the lower plot in Figure M-8 is compared with Figure M-9, which depicts condensation rates on the drift walls for a poorly ventilated drip shield.

Comparison of the Porous-Medium and Network Models–Both the porous-medium model and the network model show that much of the water evaporated from the host rock around the emplacement drifts condenses on the drift walls in the unheated parts of the drift (i.e., the exhaust standoff and the access turnout areas). The porous-medium model includes full coupling of heat and mass flow between the host rock and the drift opening and extends over the entire regulatory time period, but it is not well suited to modeling each waste package in an entire emplacement drift and provides only a limited representation of convective processes in the gas phase. To address these limitations, computational fluid dynamic calculations are used to develop effective dispersion coefficients that represent gas-phase transport, and the condensation network model represents many waste packages as well as the unheated parts of a drift. The porous-medium model and the network model generate comparable results in terms of the onset time, location, and magnitude of condensation, although the porous-medium model predicts most condensation to occur within the near-field host rock.

Condensation anywhere in heated parts of the drift depends on the local temperature and vapor pressure. These state variables correlate strongly to porous-medium flow processes (vapor pressure lowering and capillary pumping) and the axial transport of water vapor in the open drift environments. These processes, ideally represented by a fully coupled approach, have been captured by the assumptions inherent to the porous-medium and network model approaches. Condensation under the drip shield is predicted only by the network model using bounding approximations and depends on the location of evaporation within the invert. Local thermal-hydrologic conditions that would be consistent with the possibility of condensation under the drip shields are not predicted by the porous-medium model.

Representation for TSPA–Four cases from the condensation network model are selected to represent condensation on the drift walls in the TSPA-LA. These are the low- and high-invert transport cases for the equalized gas-phase composition across the drip shield using the high and low axial dispersion coefficients. These choices include bounding conditions and maximize the rate of condensation on the drift wall. A detailed description of the modeling abstraction for the network model can be found in *In-Drift Natural Convection and Condensation Model* (BSC 2003a, Section 6.3). In the TSPA-LA, condensate that forms at the drift wall is treated like seepage so that all of it drips onto the drip shield and has the same effect on transport processes in the invert and coupling of transport to the host rock.

M.4.3 Screening of Condensation under the Drip Shield

Breach of the waste packages or drip shields (facilitating advective transport) relies on uniform or localized corrosion (BSC 2003b; BSC 2003c). General corrosion for both the drip shield and waste package, and localized corrosion of the waste package, are implemented in TSPA-LA, with rates derived from immersed samples. The uniform corrosion rates are insensitive to solution composition for dilute conditions, so the presence of condensate has no effect. Localized corrosion of the waste package is sensitive to increased chloride concentration and lower pH values, conditions that tend to be mediated by dilution with condensate. Mildly acidic

conditions are possible with very dilute condensate in contact with gas-phase CO_2; however, localized corrosion of Alloy 22 (UNS N06022) is not likely under such dilute conditions.

With respect to transport, condensation on the underside of the drip shield is considered most likely to occur on the sides, as opposed to the crown, due to the generally warmer temperatures at the crown of the drip shield. In addition, condensation on the smooth underside will tend to cling to the drip shield and not drip onto the waste package. The occurrence of condensate on the underside of the drip shield is, therefore, considered highly unlikely to result in dripping onto underlying waste packages. Processes that limit the amount of condensation under the drip shield and further limit the fraction of that water that could contact the waste forms and contribute to advective transport, as described in the previous paragraphs, serve to significantly reduce the probability of condensation on the underside of the drip shield. In addition, because the presence of condensate is not correlated with waste package corrosion, any dripping that may occur is expected to be located independently from breaches in the waste package, thus further limiting the consequences of any condensate dripping from the underside of the drip shield (BSC 2004a, Section 6.2.41).

M.4.4 Responses to GEN 1.01 (Comments 5 and 16)

M.4.4.1 Specific Response and Basis for GEN 1.01 (Comment 5)

Condensation under the drip shields and on the drift walls was excluded from the TSPA for the site recommendation. Since that time, additional modeling, as described in the TEF 2.05 response, and observations of condensation in unventilated drift openings at Yucca Mountain have led to better understanding of the potential effects on repository performance. Condensation on the drift walls is now recognized as the most likely and volumetrically important aspect of possible condensation and is included in TSPA-LA, along with more complete representation of waste package degradation mechanisms that could occur under intact drip shields. Condensation under the drip shield remains excluded on the basis that it is chemically dilute and does not accelerate any of these mechanisms and is volumetrically limited such that, in the event of waste package breach from other causes, waste form degradation and radionuclide release are not increased significantly.

M.4.4.2 Specific Response and Basis for GEN 1.01 (Comment 16)

Observations from the Enhanced Characterization of the Repository Block (ECRB) bulkhead test have confirmed that unventilated, closed drifts produce relative humidity close to 100%. Water samples collected from various locations in the ECRB show that condensation is the predominant source (the basis for this statement is discussed in *Technical Basis Document No. 3: Water Seeping into Drifts*). The ECRB observations have also confirmed that potentially significant amounts of water can be transported and condensed in association with small differences in rock temperature (on the order of a few degrees Celsius) and that this can result from small power sources in the drift acting over months or years. Measurements of hydrologic variables are ongoing in the ECRB bulkhead test as artificial heat sources are being eliminated, so that the ambient background conditions can be observed. Importantly, the test results show that the rate of moisture transport and condensation in repository drifts is potentially significant throughout the regulatory period, starting when individual waste package locations cool to below

boiling (96°C). To address this potentially significant source of water, model calculations have been performed to evaluate the conditions for onset of condensation and the magnitude in the emplacement drift environment. The results are summarized in the TEF 2.05 response.

M.5 REFERENCES

M.5.1 Documents Cited

BSC (Bechtel SAIC Company) 2003a. *In-Drift Natural Convection and Condensation Model.* MDL-EBS-MD-000001 REV 00A, Draft. Las Vegas, Nevada: Bechtel SAIC Company. ACC: MOL.20031212.0020.

BSC 2003b. *General Corrosion and Localized Corrosion of the Drip Shield.* ANL-EBS-MD-000004 REV 01. Las Vegas, Nevada: Bechtel SAIC Company. ACC: DOC.20030626.0001.

BSC 2003c. *General Corrosion and Localized Corrosion of Waste Package Outer Barrier.* ANL-EBS-MD-000003 REV 01, with errata. Las Vegas, Nevada: Bechtel SAIC Company. ACC: DOC.20030916.0010; DOC.20031222.0002; DOC.20031222.0001.

BSC 2004a. *Engineered Barrier System Features, Events, and Processes.* ANL-WIS-PA-000002 REV 03A. Las Vegas, Nevada: Bechtel SAIC Company. ACC: MOL.20040721.0240.

BSC 2004b. *Multiscale Thermohydrologic Model*. ANL-EBS-MD-000049 REV 02B. Las Vegas, Nevada: Bechtel SAIC Company. ACC: MOL.20040720.0186.

BSC 2004c. *Drift-Scale Coupled Processes (DST and TH Seepage) Models.* MDL-NBS-HS-000015 REV 01A. Las Vegas, Nevada: Bechtel SAIC Company. ACC: MOL.20040712.0194.

Fluent 2001. *Fluent 6.0 User's Guide, Nomenclature, Bibliography & Index.* Five volumes. Lebanon, New Hampshire: Fluent. TIC: 254880.

Nitao, J.J. 1998. *Reference Manual for the NUFT Flow and Transport Code, Version 2.0*. UCRL-MA-130651. Livermore, California: Lawrence Livermore National Laboratory. ACC: MOL.19980810.0391.

Reamer, C.W. and Gil, A.V. 2001. Summary Highlights of NRC/DOE Technical Exchange and Management Meeting of Range on Thermal Operating Temperatures, September 18-19, 2001. Washington, D.C.: U.S. Nuclear Regulatory Commission. ACC: MOL.20020107.0162.

Reamer, C.W. and Williams, D.R. 2001. Summary Highlights of NRC/DOE Technical Exchange and Management Meeting on Thermal Effects on Flow. Meeting held January 8-9, 2001, Pleasanton, California. Washington, D.C.: U.S. Nuclear Regulatory Commission. ACC: MOL.20010202.0095 through MOL.20010202.0108.

M.5.2 Data, Listed by Data Tracking Number

LL040703223122.050. Validation of the Multiscale Thermal-Hydrologic Model (MSTHM) against a Corresponding Three-Dimensional Monolithic Thermal-Hydrologic Model. Submittal date: 07/14/2004.

INTENTIONALLY LEFT BLANK